Analysis of Range Measurements From a Pulsed Airborne CO_2 Integrated Path Differential Absorption Lidar

Axel Amediek, Xiaoli Sun, *Member, IEEE*, and James B. Abshire, *Senior Member, IEEE*

***Abstract*—Determining the CO_2 column abundance from an integrated path differential absorption (IPDA) lidar requires accurate knowledge of the range to the scattering surface, i.e., the column height. We have adapted and tested a ranging algorithm for the airborne IPDA CO_2 lidar designed at the NASA Goddard Space Flight Center, and have evaluated its accuracy and precision. We applied a quasi-maximum-likelihood method, using cross correlation, to estimate the range from the lidar's 1-μs-wide echo pulses. The objective was to show that the use of these temporally long laser pulses allows the determination of the optical path length with required precision. We analyzed airborne measurements made in August 2009 over the Chesapeake Bay near the Eastern Shore of Virginia. The results indicate a ranging precision of better than 3 m, which is sufficient for airborne and space-based retrievals of CO_2 column concentration.**

***Index Terms*—Carbon dioxide, integrated path differential absorption (IPDA), lidar, ranging.**

I. Introduction

ALTHOUGH increasing atmospheric CO_2 is widely accepted as the largest anthropogenic factor causing climate change, there is considerable uncertainty about its global budget. Accurate measurements of tropospheric CO_2 mixing ratios are needed to study CO_2 emissions and exchange with the land and oceans. To be useful in reducing uncertainties about carbon sources and sinks, the atmospheric CO_2 measurements need degree-level spatial resolution and $\sim$0.3% precision [1], [2]. This is difficult for passive spectrometers using reflected sunlight, particularly due to scattering from atmospheric aerosols and poor coverage at high latitudes [3]–[5]. To meet these needs, the U.S. National Research Council's 2007 Decadal Survey for Earth Science recommended a new space-lidar-based mission called "Active Sensing of CO_2 Emission Over Nights, Days, and Seasons" (ASCENDS) [6].

Manuscript received August 2, 2011; revised January 20, 2012 and May 31, 2012; accepted July 23, 2012. This work was supported in part by the National Aeronautics and Space Administration (NASA) Earth Science Technology Office's Instrument Incubator Program, by the NASA Active Sensing of CO_2 Emission Over Nights, Days, and Seasons Definition Program, and by the Goddard Space Flight Center Internal Research and Development program. The work of A. Amediek was supported by the German Aerospace Center (DLR) under Forschungssemester Grant.

A. Amediek is with the Institut für Physik der Atmosphäre, Deutsches Zentrum für Luft- und Raumfahrt, 82234 Wessling, Germany (e-mail: axel.amediek@dlr.de).

X. Sun and J. B. Abshire are with the Solar System Exploration Division, NASA Goddard Space Flight Center, Greenbelt, MD 20771 USA (e-mail: xiaoli.sun-1@nasa.gov; james.b.abshire@nasa.gov).

Digital Object Identifier 10.1109/TGRS.2012.2216884

The integrated path differential absorption (IPDA) lidar technique utilizes the strong backscatter from hard targets, or the Earth's surface, to measure the column-integrated gas absorption. Since these strong signals help minimize the laser power needed to attain high signal-to-noise ratios (SNRs) from long distances, this approach was recommended to attain the high precisions needed for the ASCENDS mission.

Since CO_2 is distributed along the path, IPDA lidar measurements depend on accurate estimates of both the differential optical depth and the column length, or range to the scattering surface. For airborne measurements at nadir, when the relative vertical variability in the CO_2 mixing ratio is small, the column density's change with range is about -0.02%/m for measurements at a 6-km altitude. For CO_2 column density estimates from space which are accurate to $< 1\%$, the IPDA lidar's range uncertainty needs to be better than 3–10 m (depending on other contributors in an overall error budget) [7]. In order to minimize instrument complexity, it is desirable to use the laser signal transmitted for the gas absorption measurements to also make the ranging measurements by retrieving the laser pulse time of flight. By this means, additional hardware for the range determination is not required.

This paper presents a practical approach for the ranging retrieval and discusses the ranging performance of an airborne IPDA lidar. The special characteristic of this system is its long laser pulsewidth of 1 μs (150 m), which is much larger than the required ranging precision. This airborne lidar first flew in fall 2008 on the National Aeronautics and Space Administration (NASA) Glenn Research Center (GRC) Lear-25 aircraft [8]. In the following sections, a description of the lidar system is given as well as a description of the applied range estimation approach. The analysis and results presented in this paper use data from flights performed in 2009.

II. IPDA Lidar Approach

NASA Goddard Space Flight Center (GSFC) has been developing a pulsed direct detection lidar approach as a candidate for the ASCENDS mission [8], [9]. The approach is a dual-band pulsed laser absorption spectrometer utilizing the IPDA lidar technique. One transmitter operates in the oxygen A-band, and the other operates in the 1575-nm absorption band of CO_2. Only the latter is addressed in the investigation presented here. The IPDA technique is used for open-path laser absorption spectroscopy measurements [10], [11] where a scattering target

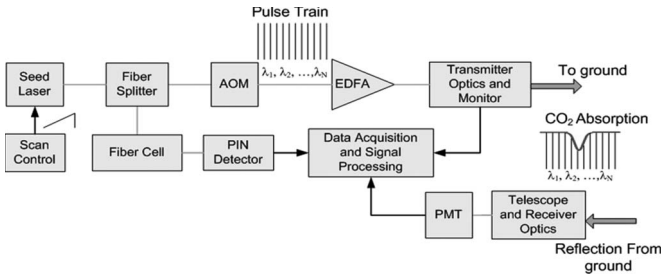

Fig. 1. Block diagram of NASA Goddard's airborne CO_2 IPDA lidar.

(such as the ground, an ocean surface, or cloud tops) is used to reflect laser light at the end of the path. By measuring the target range and the differential optical depth of the gas absorption line and by knowing the difference in the gas absorption cross sections, one can solve for the path-integrated number density of the gas molecules.

The NASA GSFC approach steps the wavelength of a laser across the selected CO_2 absorption line, and the backscatter signals are measured at each wavelength. The method of sampling an absorption line at discrete points gives information not only about the absorption strength but also about the line shape. It also allows instrumental characteristics, such as wavelength-dependent responses and/or wavelength offsets to be determined. Using pulsed lasers and time-resolved detector allows the receiver to record the full laser backscatter profiles. This enables the postdetection signal processing to isolate the laser echo signals from the surface, to measure the distance to the surface along the laser line of sight, and to discriminate laser photons scattered from the atmosphere, aerosol layers, or clouds, which arrive earlier [8]. Hence, it allows isolating the full column measurement from potential bias caused by atmospheric scattering [5]. It also substantially improves the receiver's SNR by reducing the amount of noise from the detector and the solar background.

III. Airborne CO_2 Lidar Description

In 2009, a developmental version of the CO_2 lidar was flown on the NASA GRC Lear-25 aircraft. The block diagram for the lidar is shown in Fig. 1, and its specifications are listed in Table I. The lidar's seed signal source is a distributed feedback laser diode, which is operated near 1572.33 nm by controlling its temperature and current. A ramp from a signal generator was used to sweep the current to the diode laser and, hence, its output wavelength. The diode's continuous wave (CW) output is then gated into rectangular pulses using an acousto-optic modulator, and the pulse power is amplified by an erbium-doped fiber amplifier.

A small percentage of the CW seed laser output is split off and directed through a fiber-coupled CO_2 absorption cell to a pin photodetector. The CO_2 cell serves as a monitor for center wavelength of the sweep.

The laser output is a sequence of 1-μs-wide laser pulses with an almost rectangular shape, which occur at a 10-kHz rate. The wavelength sweep of the seed laser causes the output laser pulses to step in wavelength. Here, one sweep contains 20 wavelength steps to sample the CO_2 absorption line. Fig. 2 shows an expanded view of a single laser pulse as well as a sample of the laser diode wavelength sweep through the CO_2 cell together with the 20 transmitted laser pulse amplitudes.

The collimated transmitted laser output exits through Lear-25's nadir window. The laser backscatter is collected by the receiver's 20-cm-diameter Cassegrain telescope, which views

TABLE I
Parameters of NASA GSFC's 2009 Pulsed Airborne CO_2 Lidar

Parameter	Value
CO_2 line center wavelength	1572.33 nm (typically)
Laser min & max wavelengths	1572.29 nm, 1572.39 nm
Laser wavelengths steps across absorption line	20 (for these flights)
Laser peak power/energy per pulse	25 W /25 μJ
pulse width	1 μsec
divergence	100 μrad (for these flights)
Seed laser diode type	Fitel FOL15DCWD
Laser Pulse Modulator (AOM)	NEOS Model: 26035-2-155
Fiber coupled CO_2 cell	80 cm path, 267 hPa pressure
Fiber Laser Amplifier (EDFA)	IPG EAR-10K-1571-LP-SF
Laser line scan rate	450 Hz
Laser linewidth	15 MHz
Telescope diameter	20 cm
Receiver FOV diameter	200 μrad
Receiver optical bandwidth	800 pm
Detector PMT type	Hamamatsu H10330A-75
quantum efficiency	2% (this device)
dark count rate	about 500 kHz
Receiver signal processing	Photon counting/histogramming
Histogramm time bin width	8 ns
Receiver integration time	0.9 s per readout
Recording duty cycle	45% (0.9 s every 2s)

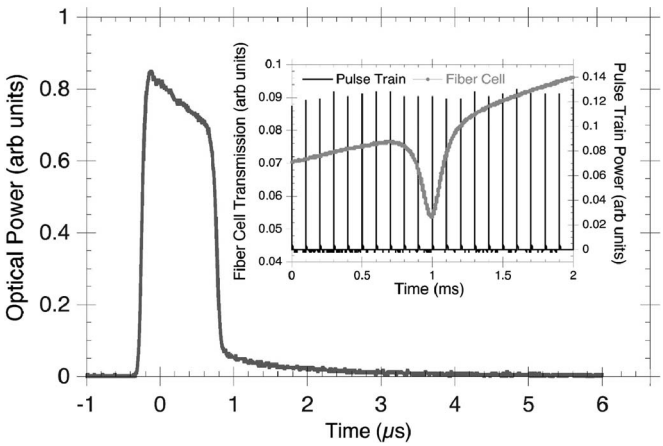

Fig. 2. (Main panel) Typical single laser pulse from the airborne laser transmitter. The pulse shape shows a decrease in pulse amplitude over the pulse interval as the fiber amplifier gain is depleted. The 1-μs-wide part of the laser pulse contains over 90% of the pulse energy. (Embedded panel): (Gray trace and left-hand axis) Sample CW wavelength scan of the diode laser (before the modulator) through the instrument's internal pressure CO_2 cell, showing CO_2 absorption and the seed laser power variability versus wavelength. (Black trace and right-hand axis) Detected laser output power versus time from the laser transmitter's power monitor.

nadir through the same window in a bistatic configuration. A multimode fiber is used to couple the received optical signal from the telescope focal plane to the detector assembly. After passing through an optical bandpass filter, the received laser pulses are focused onto a photomultiplier tube (PMT) detector. The electrical pulse output from the PMT is amplified and passed through a threshold detector, so that each output pulse represents a single detected photon. For the operating voltage and discriminator threshold used in the 2009 flights, the PMT had a photon-counting efficiency of $\sim$2%.

The receiver electronics bins the time of detected photons at 8-ns intervals to a histogram of a 2-ms time span (corresponds to one wavelength sweep), integrates these for 450 wavelength sweeps every 0.9 s, and transfers the data to the instrument computer. The bin size and integration time were chosen for satisfactory CO_2 absorption measurements and within the hardware limit of data transfer rate and storage volume of the airborne instrument. The aircraft's position and altitude data are also collected from the instruments GPS receiver, and the airplane navigation data were also recorded.

IV. Time-of-Flight Estimates

Time of flight of the laser pulses gives a direct estimate of range to the scattering surface independent of the laser pointing angle and the airplane pitch and yaw angles. Given the limited peak power available from the laser transmitter, a relatively wide (1 μs) laser pulsewidth was used to achieve the required laser pulse energy for the CO_2 absorption measurements. However, this pulsewidth corresponds to $\sim$150 m in range, which is about 100 times the required ranging precision. There is considerable interest in ranging algorithms that can estimate the laser pulse time of flight to $\sim$1% of the pulsewidth at the expected SNR.

Approaches to measure laser pulse time of flight have been studied extensively (for example, see [12]–[17]). One technique to estimate the laser pulse time of flight is the so-called early–late gate or split-gate method [18], in which the histogram of the received photons about the received pulse is split (or gated) into two segments. The number of the photons within the "early gate" is compared to that within the "late gate" through an iterative process until the numbers of photons within the early and late gates are equal. Although this is a simple algorithm, the method is not suitable for our CO_2 lidar because the laser pulse shape is usually asymmetric. Another method is to fit the received signal to an expected laser pulse shape function via a minimum least square error curve fit. However, this method requires prior knowledge of the received laser pulse shape and arrival times, which may not be always predictable. It becomes even more complicated when cloud returns and the surface returns are presented at the same time.

Here, we choose an approach to approximate maximum-likelihood receiver that gives near-optimal performance and is relatively easy to implement. The detected photon events can be modeled as a random point process. The maximum-likelihood estimation is to adjust the model parameters to maximize the conditional probability density function for the detected photon record [19]. The conditional probability density function given a target signal return $s(t-t_d)$ can be written as

$$\begin{aligned} p\left(\{n\}|s(t-t_d)\right) &= p\left(n_0, n_1, \ldots, n_{N-1}|s(t-t_d)\right) \\ &= p\left(n_0|s(t-t_d)\right) \cdot p\left(n_1|s(t-t_d)\right)\ldots \\ &= \prod_{k=0}^{N-1}\left[\left(s(t_k-t_d)\Delta t\right)^{n(t_k)} e^{-s(t_k-t_d)\Delta t}\right] \end{aligned} \tag{1}$$

where $\{n_k\} = \{n_0, n_1, \ldots, n_{N-1}\}$ is the number of detected photons in each range bin, t_k is the beginning time of the kth range bin, N is the total number of range bins, Δt is the range bin width, $s(t-t_0)$ is the average photon arrival rate which is proportional to the average signal and background power, and t_0 is the arrival time of the laser pulse. It was assumed that the range bin width Δt is sufficiently small that the number of detected photons in each range bin is either zero or one. The maximum-likelihood estimation searches the proper signal pulse shape function and the arrival time such that (1) achieves its maximum value ML and can be expressed as

$$\begin{aligned} ML &= \max\left\{p\left(\{n\}|s(t-t_0)\right);\ 0<t_d<T\right\} \\ &= \max\left\{\ln\left[p\left(\{n\}|s(t-t_d)\right)\right];\ 0<t_d<T\right\} \\ &= \max\left\{\sum_{k=0}^{N-1} n(t_k)\ln\left[s(t_k-t_d)\right];\ 0<t_d<T\right\} \end{aligned} \tag{2}$$

where T is the time interval to search for the target returns.

If the average background light and the signal pulse shape are known, the maximum-likelihood estimate of the laser pulse time of flight can be obtained by first calculating the cross correlation of the detected photon count sequence with the logarithm of the pulse shape function and finding the time shift at the peak value of the correlation function. For rectangular pulse shapes, (2) can be simplified as

$$\begin{aligned} ML &\approx \max\left\{\sum_{k=0}^{N-1} n(t_k)s(t_k-t_d);\ 0<t_d<T\right\} \\ &= \max\left\{\mathrm{xcorr}\left[n(t), s(t-t_d)\right];\ 0<t_d<T\right\} \end{aligned} \tag{3}$$

where $\mathrm{xcorr}[n(t), s(t-t_d)]$ is the cross-correlation function of the signal pulse shape and the received photon sequence. In this form, the signal pulse shape function is also called the kernel of the cross-correlation function. For nearly rectangular pulse shapes, (3) can still be used to estimate the laser pulse time of flight with satisfactory performance.

There are several advantages of the cross-correlation and peak searching algorithm. It does not require prior knowledge of the target range, and it gives multiple peak outputs when there are multiple targets along the laser path, such as thin clouds and ground. The algorithm always converges to give real solutions and, unlike curve fitting, requires no initial guess. It also gives a relative measure of the target reflectance based on the peak value and SNR of the cross-correlation function.

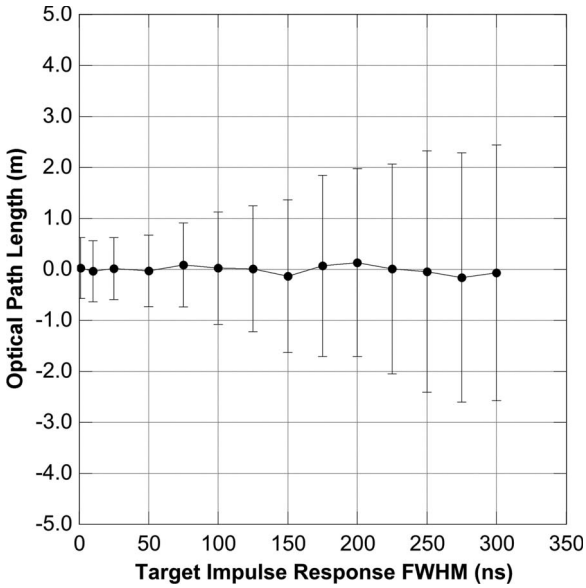

Fig. 3. Simulation results of the column height measurements using the cross-correlation and peak search technique. The mean and the standard deviation (error bar) of the column height are plotted as a function of the target impulse FWHM pulsewidth. The laser pulse shape used in the simulation was modeled to match the actual laser pulse shape shown in Fig. 4. The pulse energy was 180 detected photons per pulse, and 200 pulses were averaged for each column height measurement.

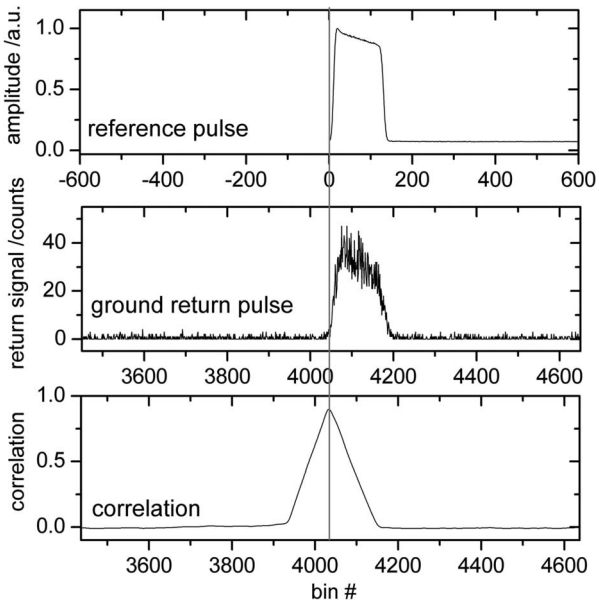

Fig. 4. Laser pulse cross-correlation ranging processing. Calculation of a cross correlation between a reference pulse and the ground return pulse. The units of the x-axis are in 8-ns bins.

As shown in Fig. 2, the transmitted laser pulses were approximately rectangular, but they had rise and fall times of about 40 ns and a tilted top due to the decreasing gain of the laser amplifier over the pulse duration. We used both the logarithm of the pulse shape and raw pulse shape as the kernel, but the results did not show significant differences. We also tried the rectangular pulse shape as the kernel but yielded slightly poor measurement precision. Using the transmitted laser pulse shape as the kernel yielded cross-correlation functions with sharper and more symmetric peaks.

One factor that can affect the performance of this measurement technique is a height-distributed target (such as trees or sloped ground) that causes spreading in the echo pulse. The pulse spreading is determined by the surface impulse response function, defined as pulse shape of the reflected signal in response to an impulse of laser illumination. The received laser pulse shape is the convolution of the transmitted laser pulse function and the target impulse response [15]. When the transmitted pulse shape is used as the kernel, the peak of the cross-correlation function becomes rounded and the measurement precision degrades slightly.

Fig. 3 shows the result of a computer simulation of the range measurements as a function of the target's impulse response. It shows that pulse spreading from the target increases the standard deviation (error bar) of the column height measurement, but has little effect on the mean. The slope effect in our airborne CO_2 lidar is negligible because of the small ($\sim$1-m diameter) laser footprint size.

For a space-based mission like ASCENDS, the pulse spreading in the lidar's recorded echo pulses will depend on several factors, including the laser's footprint size, the surface slope and roughness, presence or absence of trees, the laser pulse rate, and along-track integration distance. The laser beam divergence angle has to be sufficiently small to keep the slope effect negligible. For example, for a CO_2 lidar operating from 450-km altitude, a laser beam divergence of 100 μrad is adequate to maintain a target impulse response pulsewidth of $<$ 30-ns full-width at half-maximum (FWHM) [15] for $< 5^\circ$ surface slope. The receiver integration time has to be sufficiently short that the target range variation along the ground track is well within the error budget.

V. Ranging Methodology

In 2009, we made similar measurements over horizontal paths from the laboratory and vertically from the aircraft. For each, the column length calculations based on lidar backscatter profiles average over 0.9 s. Each of these averages contained the sum of the detected photons obtained by 450 wavelength sweeps, and each sweep contained the backscatter profiles of 20 laser pulses (corresponding to 20 wavelength steps), as described in Section II. The number of detected photons per wavelength step in the 0.9-s record varied between about 60 and 5000 depending on the flight altitude, surface reflectivity, and CO_2 absorption. We computed the cross-correlation for all 20 wavelength steps in the record (i.e., using 9000 laser pulses).

Fig. 4 shows an example of the average outgoing laser pulse shape, the histogram of received photons, and the cross correlation of the two. The laser pulse shape was determined by measuring the echo pulse shape from a flat target board and averaging it over several minutes to maximize the SNR. As expected, the shape of echo pulse histogram resembles the transmitted laser pulse shape. The airborne measurements showed that some of the received surface echoes had slightly wider pulsewidths ($< 15\%$) due to the surface slope, roughness, and elevation changes over the receiver's integration time. The time of flight is estimated as the peak location of the cross-correlation function.

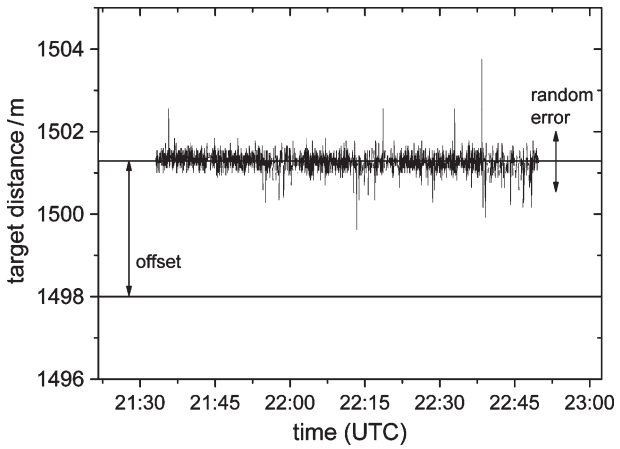

Fig. 5. Results from a series of ranging measurements from the laboratory to a flat plate target at a range of 1.5 km. The standard deviation of the range is ∼25 cm.

VI. Stationary and Airborne Ranging Measurements

The CO_2 lidar range measurements were initially made from the laboratory over a 1.5-km-long horizontal path to a fixed flat target board on a radio tower. This allows testing the algorithm and determining its precision under stationary target and constant signal level.

Fig. 5 shows the measurement results. The standard deviation of the random error around the mean value was 25 cm for a 0.9-s integration time (with an average SNR of 42). This represents the lidar's range precision for ideal conditions. The path length to the target was determined by an independent measurement, which had an uncertainty of ±1.5 m. An offset of about 3 m resulted using the uncalibrated retrieval algorithm.

Airborne lidar measurements were made from the NASA GRC Lear-25 on several ASCENDS sponsored flights during August 2009, including a flight over the Eastern Shore of Virginia and the Chesapeake Bay on August 17. Analyzing these measurements allowed evaluating performance under flight conditions and naturally occurring backscatter conditions. Fig. 6 shows the racetrack-type flight path, where altitude increases were made during the northern turn. The segments above land and water sections captured alternately and the aircraft ascended stepwise from about 4.8 to 11.7 km above ground. Each straight-line section was about 50 km long. The water surface of the Chesapeake Bay provided a flat surface with known elevation. This allowed assessing performance of the range estimates calculated from the received lidar signal, which is discussed in the following. The aircraft altitude is also measured by an onboard GPS receiver. Generally, the mean sea surface height corresponds to the GPS datum level, if the local ellipsoid–geoid correction is considered (see Fig. 7). Thus, the actual altitude of the aircraft above the scattering surface is known here. The nearly flat bay water surface is an ideal target for comparing the lidar range estimates and GPS data, because there is no unknown variability from ground topography and vegetation. Fig. 8 shows the measurement results for a 90-min segment of the flight. When the aircraft was not turning or climbing, the lidar-measured distance closely followed the GPS

Fig. 6. (Left) Top view of the August 17, 2009, flight track (Chesapeake Bay close to Hampton, VA, USA): The same ground track (land and water) was passed five times in different flight altitudes (Source: Google Earth 2009). (Right) Side view of the flight track showing the five altitude levels (Source: Google Earth 2009).

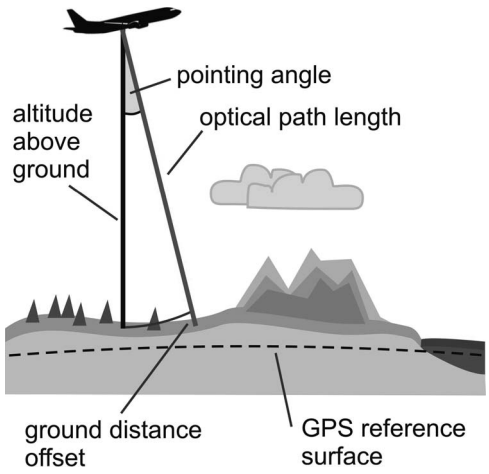

Fig. 7. Geometry of the airborne measurements including factors that influence the optical path length (column length) of the lidar.

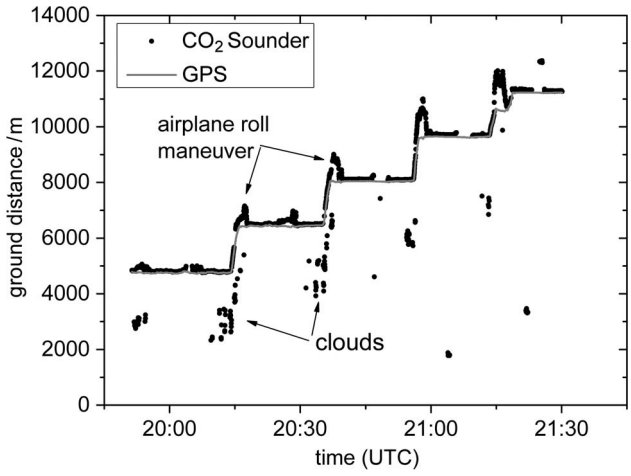

Fig. 8. (Black dots) Ranging results for the measurement flight shown in Fig. 6, derived from the lidar signal, and (gray line) airplane altitude from the GPS receiver. The time is in (hh:mm) format.

estimates. Some shorter ranges made to the top of a thin bank of clouds near the northern turn point are also evident.

VII. Analysis

When over the Chesapeake Bay's water surface during level flight, the ranging precision (random error) of the lidar can be estimated as the standard deviation of the difference between

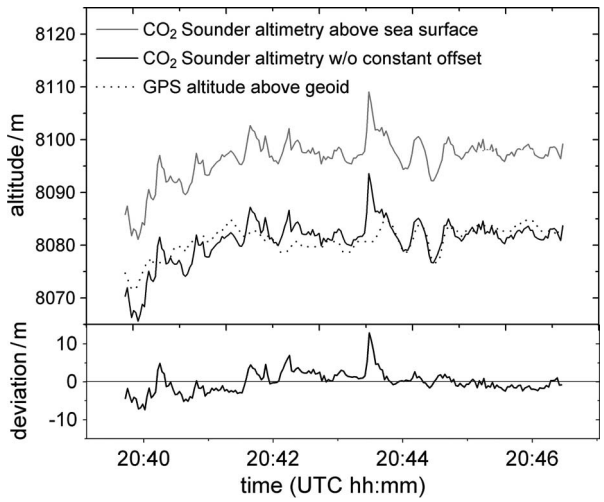

Fig. 9. Lidar measurements of range for a flight section over the Chesapeake Bay at about 8.1-km altitude. (Upper panel) Lidar and GPS data. (Lower panel) Deviation of the lidar measurements from the GPS reference, after removing a constant offset.

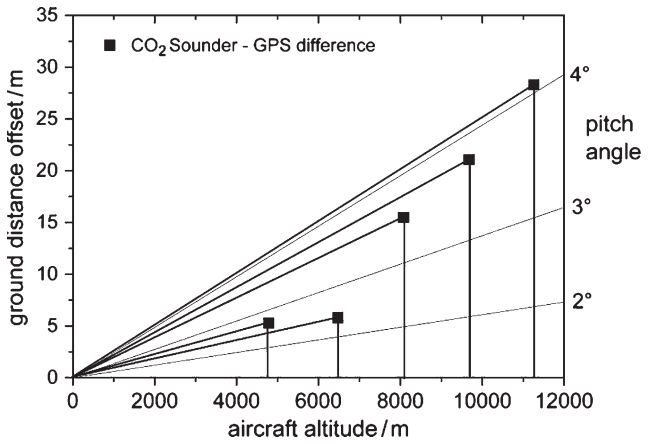

Fig. 10. Differences observed between CO_2 lidar ranging measurements and GPS receiver altitude. Squares represent mean values for the entire flight sections over the sea at each of the five flight altitude levels. Gray lines indicate calculated ground distance offsets caused by various aircraft pitch angles.

the lidar ranging (laser pulse time-of-flight measurement) and the GPS altitude readings. Fig. 9 shows both the the lidar results (gray) and the GPS data (dotted) for one segment of the flight path over the water surface (0.9-s receiver integration time). The black line corresponds to the offset-corrected lidar data. The lower panel shows the deviation of the offset-corrected lidar data from the GPS data. The resulting standard deviation between GPS and the lidar was 2.8 m for SNRs between 21 (online) and 49 (offline). As expected, the range standard deviations in flight are higher than those for the stationary measurements.

An analysis was also made for ranging bias. This used the average difference between the derived lidar range and the airplane altitude from the GPS receiver, each calculated for the five flight legs over the bay. The results, shown in Fig. 10, show a generally increasing range offset with aircraft altitude. The trend of the range offset can be explained by the geometry of the aircraft's pitch angle and the laser beam's angle to the surface, which is shown in Fig. 7 as the ground distance offset. The dashed lines in Fig. 10 indicate the calculated introduced ground distance offset vs. flight altitude for different laser beam off-nadir angles between 2.4° and 4.1°. Discussions with the pilots indicated that, for aircrafts, like the Lear-25, the pitch angles increase with ascending flight altitude typically in the range between about 2° and 4.5°. Except for a few meters, all the range offset can be explained by the mentioned geometrical effect in combination with the change of the aircraft's pitch angle, during cruise at 4800 to 11 700 m altitude.

VIII. Residual Flight Ranging Errors

For flight measurements, several factors impact the random error in the range estimates. These include the laser pulse broadening by the slope and roughness of the backscattering surface and by the surface height's variation over the receiver's integration time, as well as the noise on the echo pulse signal caused by background noise and finite number of detected signal photons, and the signal sampling error.

The validation of the measured IPDA column length by comparing it to the aircraft's GPS altitude is impacted by some additional factors besides the GPS receiver uncertainty: In general, the aircraft's altitude above ground is shorter than the laser path length, because the lidar system is not pointed exactly in nadir direction (see Fig. 7), and the aircraft changes its pitch and roll angles during flight. The laser beam pointing angle with respect to the airplane body is fixed, but airplane pitch angle changes with speed and altitude. Unfortunately, the actual aircraft attitude data were not available for this work, which made it difficult to compare absolute range measurements. In spite of the mentioned factors, the measured data showed that we can achieve an rms ranging precision of 2.8 m compared to the altitude from an onboard GPS receiver, which is adequate for a CO_2 IPDA lidar. Future investigations on the ranging performance should include aircraft attitude data to help correct for the geometrical effects, which is expected to reduce the methodical differences between lidar ranging and GPS altitudes.

IX. Summary

This work has assessed the ranging performance of the airborne NASA GSFC pulsed CO_2 IPDA lidar. For CO_2 column density measurements applying the IPDA lidar technique, it is essential to know the column length that corresponds to the laser line-of-sight range to the scattering surface. This information can be retrieved by determining the laser pulse time of flight from the measured signal. The laser pulselength generated by this system is 1 μs, corresponding to 150 m, which is much higher than the required precision being on the order of some meters. The results showed that a cross-correlation peak detection algorithm was robust and gave adequate ranging precision. A major advantage is that it does not require any prior information about the range. The lidar's ranging precision was measured to be 0.25 m to a stationary target over a 1.5-km-long horizontal path length. Airborne measurements, made in August 2009 over the Chesapeake Bay, allowed the ranging precision to be assessed by comparing to GPS data, and the standard deviation was better than 3 m. The major sources

of the scatter in the difference between the airborne ranging measurements and GPS readings are likely due to the SNR, variations in aircraft attitude, and GPS receiver uncertainty. An observed altitude-dependent offset between the lidar's estimate of range and the GPS data can be largely explained by the geometry of the off-nadir pointing of the laser beam caused by the airplane pitch angle, which can be taken into account in future ranging investigations. In summary, the results have shown that the 2009 configuration of the CO_2 IPDA lidar can achieve a ranging precision, which is adequate for column CO_2 density estimates, without a separate ranging channel and associated additional hardware.

ACKNOWLEDGMENT

The authors would like to thank other members of the NASA Goddard Space Flight Center CO_2 integrated path differential absorption lidar team, particularly H. Riris, B. Hasselbrack, and G. Allan.

REFERENCES

[1] P. P. Tans, I. Y. Fung, and T. Takahashi, "Observational constraints on the global atmospheric CO_2 budget," *Science*, vol. 247, no. 4949, pp. 1431–1438, Mar. 1990.

[2] S. Fan, M. Gloor, J. Mahlman, S. Pacala, J. Sarmiento, T. Takahashi, and P. Tans, "A large terrestrial carbon sink in North America implied by atmospheric and oceanic carbon dioxide data and models," *Science*, vol. 282, no. 5388, pp. 442–446, Oct. 1998.

[3] S. Houweling, W. Hartmann, I. Aben, H. Schrijver, J. Skidmore, G.-J. Roelofs, and F.-M. Breon, "Evidence of systematic errors in SCIAMACHY-observed CO_2 due to aerosols," *Atmos. Chem. Phys.*, vol. 5, no. 11, pp. 3003–3013, Nov. 2005.

[4] M. Buchwitz, R. de Beek, J. P. Burrows, H. Bovensmann, T. Warneke, J. Notholt, J. F. Meirink, A. P. H. Goede, P. Bergamaschi, S. Körner, M. Heimann, and A. Schulz, "Atmospheric methane and carbon dioxide from SCIAMACHY satellite data: Initial comparison with chemistry and transport models," *Atmos. Chem. Phys.*, vol. 5, no. 4, pp. 941–962, Mar. 2005.

[5] I. Aben, O. Hasekamp, and W. Hartmann, "Uncertainties in the space-based measurements of CO_2 columns due to scattering in the Earth's atmosphere," *J. Quant. Spectrosc. Radiat. Transfer*, vol. 104, no. 3, pp. 450–459, Apr. 2007.

[6] NASA ASCENDS Mission Science Definition and Planning Workshop Report, 2008. [Online]. Available: http://cce.nasa.gov/ascends/12-30-08%20ASCENDS_Workshop_Report%20clean.pdf

[7] "A-SCOPE, Advanced Space Carbon and Climate Observation of Planet Earth, Report for Assessment, SP-1313/1," Eur. Space Agency, Noordwijk, Netherlands, 2008.

[8] J. B. Abshire, H. Riris, G. R. Allan, C. J. Weaver, J. Mao, X. Sun, W. E. Hasselbrack, S. R. Kawa, and S. Biraud, "Pulsed airborne lidar measurements of atmospheric CO_2 column absorption," *Tellus B*, vol. 62, no. 5, pp. 770–783, Nov. 2010.

[9] J. B. Abshire, H. Riris, G. R. Allan, C. J. Weaver, J. Mao, X. Sun, W. E. Hasselbrack, A. Yu, A. Amediek, Y. Choi, and E. V. Browell, "A lidar approach to measure CO_2 concentrations from space for the ASCENDS mission," *Proc. SPIE*, vol. 7832, pp. 78320D-1–78320D-3, Oct. 2010.

[10] R. Measures, *Laser Remote Sensing: Fundamentals and Applications*. New York: Krieger Publ., 1992.

[11] J. Caron and Y. Durand, "Operating wavelengths optimization for a space-borne lidar measuring atmospheric CO_2," *Appl. Opt.*, vol. 48, no. 28, pp. 5413–5422, Oct. 2009.

[12] I. Bar-David, "Communication under the Poisson regime," *IEEE Trans. Inf. Theory*, vol. IT-15, no. 1, pp. 31–37, Jan. 1969.

[13] I. Bar-David, "Minimum-mean-square-error estimation of photon pulse delay," *IEEE Trans. Inf. Theory*, vol. IT-21, no. 3, pp. 326–330, May 1975.

[14] M. Elbaum and P. Diament, "Estimation of image centroid, size and orientation with laser radar," *Appl. Opt.*, vol. 16, no. 9, pp. 2433–2437, Sep. 1977.

[15] C. S. Gardner, "Target signatures for laser altimeters: An analysis," *Appl. Opt.*, vol. 21, no. 3, pp. 448–453, Feb. 1982.

[16] C. S. Gardner, "Ranging performance of satellite laser altimeters," *IEEE Trans. Geosci. Remote Sens.*, vol. 30, no. 5, pp. 1061–1072, Sep. 1992.

[17] J. L. Bufton, "Laser altimetry measurements from aircraft and spacecraft," *Proc. IEEE*, vol. 77, no. 3, pp. 463–477, Mar. 1989.

[18] H. C. Salwan, "Error analysis of optical range measurement systems," *Proc. IEEE*, vol. 58, no. 10, pp. 1741–1745, Oct. 1970.

[19] D. L. Snyder, *Random Point Processes*. New York: Wiley, 1975.

Axel Amediek was born in Munich, Germany, on June 17, 1975. He received the Diploma in physics from the Technische Universität München, Munich, in 2001, and the Ph.D. degree from the Ludwig-Maximilians-Universität, Munich, in 2007. As a Ph.D. student, he joined the Institut für Physik der Atmosphäre, Deutsches Zentrum für Luft und Raumfahrt (DLR, the German Aerospace Center), Wessling, Germany, where his topic was the development of a laboratory prototype of an integrated path differential absorption (IPDA) lidar system for the measurement of atmospheric CO_2.

In 2009, he received the DLR Forschungssemester Grant supporting his scientific visit with the NASA Goddard Space Flight Center, Greenbelt, MD, as a Postdoctoral Research Fellow. Since 2007, he has been a Research Associate with the Institut für Physik der Atmosphäre, DLR, and continued his work with focus on airborne lidar systems for CO_2 and methane. He is currently involved in the development of the DLR airborne demonstrator for future space-based IPDA lidars for greenhouse gases (such as MERLIN).

Xiaoli Sun (S'88–M'90) was born in Beijing, China. He received the B.E. degree from Taiyuan Institute of Technology, Taiyuan, China, in 1982 and the M.S.E. and Ph.D. degrees in electrical engineering from Johns Hopkins University, Baltimore, MD, in 1985 and 1989, respectively.

Since 1999, he has been with the NASA Goddard Space Flight Center (GSFC), Greenbelt, MD, where he is currently a Senior Scientist with the Laser Remote Sensing Laboratory, Solar System Exploration Division. He was the Lead Engineer in photodetector development and receiver performance analysis for the Mars Orbiter Laser Altimeter on the Mars Global Surveyor mission launched in 1996 and the Geoscience Laser Altimeter System on the Ice, Cloud and land Elevation Satellite mission launched in 2003. He was the Instrument Scientist for the Mercury Laser Altimeter on the Mercury Surface, Space Environment, Geochemistry and Ranging mission launched in 2004 and the Lunar Orbiter Laser Altimeter on the Lunar Reconnaissance Orbiter mission launched in 2009. He is involved in many lidar developments at GSFC, NASA, in the areas of instrument design and performance analysis for future NASA missions, such as the CO_2 lidar for Active Sensing of CO_2 Emission Over Nights, Days, and Seasons mission and the swath-mapping lidar for the Lidar Surface Topography mission.

Dr. Sun is a member of the Optical Society of America.

James B. Abshire (S'73–M'81–SM'85) was born in Knoxville, TN, on December 6, 1951. He received the B.S. degree in electrical engineering from the University of Tennessee, Knoxville, in 1974 and the Ph.D. degree in electrical engineering from the University of Maryland, College Park, in 1982.

He is the Senior Scientist for laser sensing with the Solar System Exploration Division, NASA Goddard Space Flight Center, Greenbelt, MD. He has helped lead the development of space lidar at Goddard and was Instrument Scientist on the Mars Orbiter Laser Altimeter on the Mars Global Surveyor mission and the Geoscience Laser Altimeter System on the ICESat mission. He currently is leading Goddard's work in remotely measuring atmospheric CO_2 with lidar and serves on the formulation teams for the NASA Active Sensing of CO_2 Emission Over Nights, Days, and Seasons (ASCENDS) mission and the French/German MERLIN mission.

Dr. Abshire is a member of the Optical Society of America, American Geophysical Union, and European Geophysical Union. He is serving as Cochair of the lidar working group in the Instrumentation and Future Technologies Technical Committee of the IEEE Geoscience and Remote Sensing Society.